Advances in Science and Technology Research Journal

Advances in Science and Technology Research Journal, 2026, 20(4), 328–346
https://doi.org/10.12913/22998624/215234
ISSN 2299-8624, License CC-BY 4.0

Received: 2025.10.22
Accepted: 2026.02.15
Published: 2026.03.01

Exploring the impact of carbon fiber reinforced polymer material parameters on energy absorption and collision performance: Design and evaluation

Nguyen Phi Truong[1], Le Duc Hieu[1], Kien Trung Nguyen [1], Thanh Cong Nguyen[2*], Lu Duc Thanh Vinh[2]

[1] Faculty of Transportation Engineering, School of Mechanical and Automotive Engineering, Hanoi University of Industry, Hanoi, Vietnam
[2] Faculty of Mechanical Engineering, University of Transport and Communications, Hanoi, Vietnam
* Corresponding author's e-mail: congnt@utc.edu.vn

ABSTRACT

In today's era, transportation has become an integral and indispensable part of daily life. Traffic safety is a top priority worldwide to reduce accidents and damage to both people and property. Research and development of safety systems are becoming increasingly important, and there has been recent progress in the design of energy-absorbing crash boxes in origami shapes made from carbon fiber reinforced polymer (CFRP) materials. This study first identifies an optimal origami-shaped crash box geometry made of CFRP, and then systematically investigates the impact of CFRP material parameters (layer orientation angles and thickness) on its energy absorption and collision performance. Using the Taguchi method in design and research, the results show that the box made of CFRP material exhibits approximately 40% higher impact resistance to an aluminum box of the same weight and dimensions. However, CFRP boxes have a maximum crushing force 2.5 times higher than aluminum. Compared to conventional square box structures using aluminum, origami structures with CFRP material also exhibit better energy absorption efficiency and lower maximum crushing force by 118%.

Keywords: origami, Taguchi, structure, CFRP.

INTRODUCTION

As society progresses, along with the development of human and economic foundations, transportation has become more convenient and necessary than ever before. With modern, advanced, and increasingly prevalent means of transportation such as automobiles, there are also inherent risks of high-speed accidents, posing significant challenges to road safety due to the high speed and large volume of vehicles in circulation. This has resulted in considerable human and vehicular casualties. Recognizing this issue, recent studies have focused on researching and designing improved protective and energy-absorbing devices to convert kinetic energy into other forms of energy to minimize damage. These protective and energy-absorbing devices must operate stably and have a repeatable deformation mode to reduce the likelihood of impact. Additionally, the produced devices must meet criteria such as being lightweight, easily replaceable, cost-effective, and capable of absorbing most of the impact force. A collision energy absorption device known as a crash energy absorption box has been developed to meet these conditions.

The crash energy absorption box appears in automobiles and is crucial for absorbing collision energy in aircraft and trains. It is part of the passive safety system, minimizing potential passenger injuries and vehicle damage in collision situations. The design of this box is expected to have good kinetic energy absorption capabilities during collisions. In the event of a head-on collision, this box will experience a significant impact force in a

very short time, leading to compression along the axis while absorbing collision energy. This helps maintain the vehicle's deceleration safely, reducing the risk of passenger injury. At this point, the box must deform against other components by absorbing maximum energy to minimize repair costs after collision damage by Hussain et al. [1].

The crash energy absorption box has a thin structure attached to the front area of the vehicle (Figure 1). The most commonly used box type is made of metals such as aluminum and steel because they are inexpensive and easy to manufacture. However, they have the drawback of having a lower specific energy absorption (SEA) value than CFRP materials by Kadarno et al. [2]. This value partly depends on the weight of the material, so reducing the weight of the crash box by using composite materials may only account for a tiny part of the overall vehicle weight. However, composite crash boxes can achieve superior results in collision energy absorption compared to existing metal crash boxes through optimal design. Despite offering these advantages, crash boxes made of composite materials are rarely used, except in high-end or Formula 1 racing cars, due to their high cost and ongoing research and development stage (Figure 2).

Ma et al. [4] conducted a comparative analysis between column-shaped and origami-shaped (diamond) crash boxes, revealing that the origami configuration can further reduce the initial peak force by approximately 13–34% relative to the column-type design, without compromising crash energy absorption efficiency. Similar findings have been reported by other researchers [5, 6], indicating that the origami geometry contributes to a reduction in initial peak force while enhancing overall crash energy absorption capability. Yuan et al. [7] demonstrated that origami-shaped crash boxes can achieve a 107.1% improvement in SEA and a reduction of up to 68.3% in peak crushing force (PCF) compared with conventional designs. Likewise, Ma and You [8] found that the origami configuration increased the average crushing force by 57.4% and lowered the initial peak force by 36.5% relative to standard square crash boxes. Collectively, these studies highlight the superior crashworthiness characteristics of origami-inspired crash energy absorbers.

CFRP, also known as carbon fiber reinforced plastic, is a lightweight reinforced polymer containing carbon fibers. It exhibits superior performance in terms of low weight and mechanical properties such as stiffness, energy, and strength capability, Sun et al. [10]. CFRP materials are relatively expensive to manufacture but are commonly used due to their exceptional properties and versatile applications across various industries such as aviation for wings, fuselage, and fan blades; automotive for body panels, chassis components, and suspension systems; and medical for prosthetic limbs and dental braces, among others. In the automotive industry, continuous efforts are made to reduce vehicle weight in order to

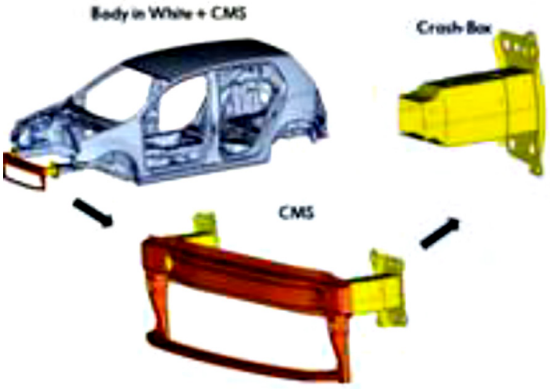

Figure 1. Position of the energy absorption box in collision [3]

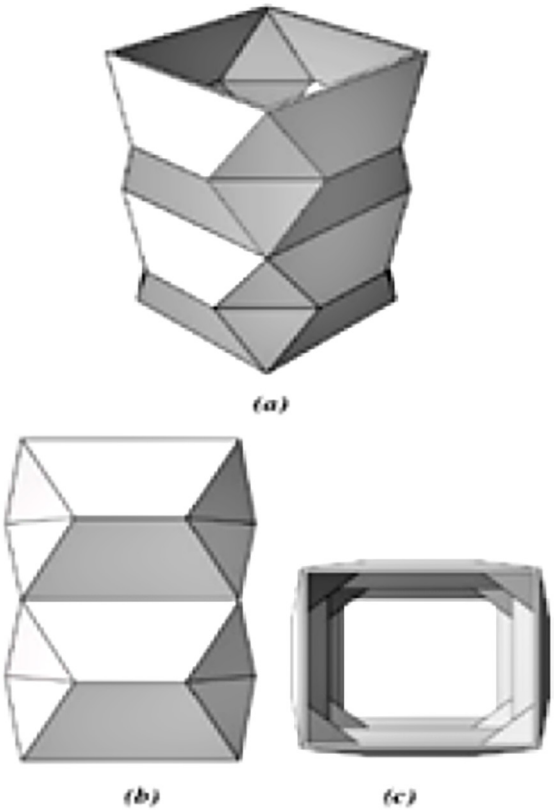

Figure 2. Origami-shaped energy-absorbing crash box [9] (a); (b); (c) – three projection views of the box

minimize raw material consumption and improve fuel efficiency. Consequently, composite polymer materials are replacing an increasing number of metallic components. Using composite materials in vehicle components aims to optimize the four factors to achieve the purpose above.

In contrast to metals, most composite materials exhibit brittle behavior instead of ductility when subjected to loading. While metallic structures fail under crushing or impact due to instability, composite materials are destroyed through fracture mechanisms involving fiber breakage, matrix cracking, and interlaminar delamination. Several studies have been conducted on crash boxes made of composite materials for impact energy absorption. Compared with alloys, metals are commonly used in vehicles; however, composite materials exhibit higher energy absorption capability. Most recently, in 2023, Kadarno and colleagues [2] conducted research on the impact resistance of crash energy absorption boxes made of CFRP, glass fiber reinforced plastic (GFRP), lightweight steel ST37, and aluminum 6061-T6. The results showed that CFRP material had superior SEA values due to its strength and lightweight. In 2017, Zhu and colleagues [11] studied cylindrical structures using aluminum, CFRP, and hybrid aluminum CFRP materials, concluding that tubes with CFRP material had the highest SEA values among the tested materials. Guangyong and associates [12] also evaluated the SEA and crushing performance efficiency (CFE) values between CFRP, aluminum, and steel tubes. The results indicated that CFRP had the two highest values among the three types. With these advantages, CFRP materials are increasingly being researched and widely used across various industries (Figure 3, 4).

Currently, research on impact energy-absorbing boxes primarily focuses on geometric cross-sectional variations such as squares, cylinders, hexagons, and octagons using the same type of material GFRP to assess force distribution and SEA by Hussain et al. [14]; altering different materials such as aluminum, steel, GFRP, CFRP using five similar geometric shapes and subjecting them to different loading orientations to evaluate SEA by Zhu et al. [11]; incorporating aluminum foam into specific locations within square impact-absorbing box cores to enhance energy absorption capability, compression and impact simulations are conducted to analyze SEA, PCF crush force, deformation modes, and protective abilities of the impact box by Wang et al. [15], or utilizing 3D printing technology to create hierarchical honeycomb structures within the box core by Tan et al. [16]. All of the research above endeavors serve the purpose of optimizing impact energy-absorbing boxes to achieve the best absorption efficiency. Although there are studies evaluating the use of CFRP in impact energy-absorbing boxes, there is a paucity of research examining the effect of geometric factors on the energy absorption efficacy of origami-shaped impact energy-absorbing boxes. Therefore, this paper will systematically investigate the influence of various parameters of composite materials on the structure's performance (Figure 5, 6).

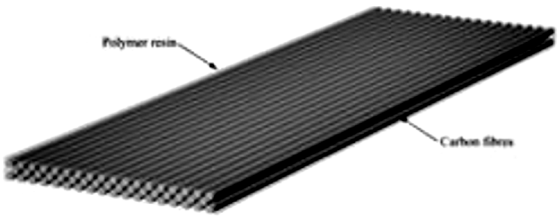

Figure 3. CFRP material [13]

THEORETICAL FOUNDATIONS, SIMULATION MODEL

Finite element method in energy absorption box simulation

The finite element method (FEM) is employed to describe problems in mechanics. This method

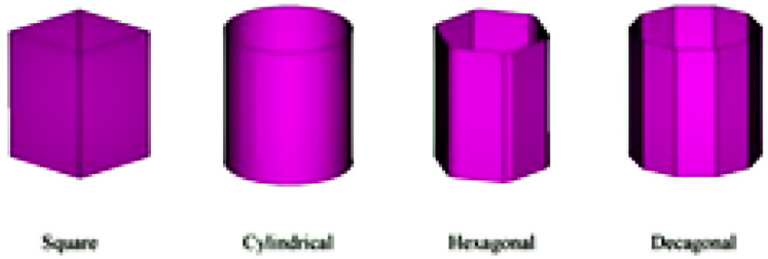

Figure 4. Various geometric shapes of impact energy absorption box [14]

Figure 5. Use of aluminum foam in impact energy absorption box [15]

has been developed to address complex issues ranging from structural mechanics and heat transfer to various fields such as construction, mechanical engineering, etc. In 1955, Argyris formulated the energy and matrix methods theorems, laying the groundwork for developing the finite element method. In 1967, Zienkiewicz and Taylor published the book marking the formal introduction of FEM in the field of structural mechanics and highlighting the concepts and methods of using FEM to solve various issues related to temperature, structural mechanics, and many other industries by Võ Như Cầu [17].

Abaqus is a leading structural simulation and analysis software developed by Dassault Systèmes SIMULIA. One of its notable features is

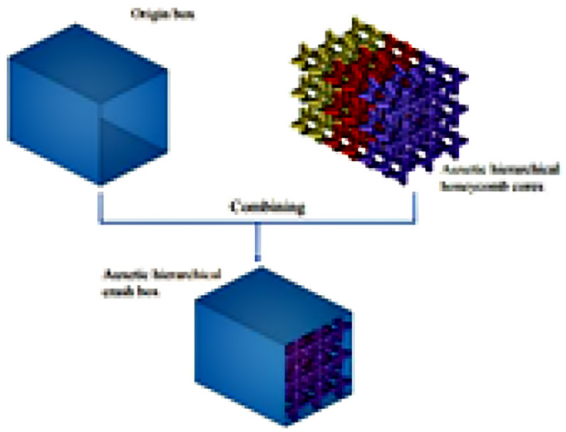

Figure 6. Hierarchical honeycomb-shaped energy absorption box [16]

the ability to integrate various types of analyses, such as static, dynamic, thermal, and heat transfer. Additionally, Abaqus assists users in the simulation and optimization of designs, helping to minimize risks and testing costs. It is widely used for static simulation, evidenced by abundant research papers utilizing Abaqus. In their 2011 study, Khalkhali et al. [18] conducted experimental and numerical studies on the static crushing response of S-shaped square tubes. Kim et al. [19] analyzed the characteristics of short square beams made of aluminum/CFRP under static lateral loading. Huyi et al. [20] simulated the static compression of rubber foam, while Quanjin et al. [21] investigated the static crushing behavior of carbon/aramid tapered tubes used as energy-absorbing components in automotive crash boxes. All these studies relied on Abaqus software for its advantages, including ease of setup, control, and provision of accurate material models reflecting the behavior of various materials under static loading conditions. This is crucial for obtaining realistic and reliable simulation results by Rabiee et al. [22]. Consequently, Abaqus has become a flexible and effective tool in research on structural behavior and impact under static loading conditions.

Taguchi optimization method

Variance analysis on data collected from Taguchi experimental designs can be utilized to select new parameter values for optimizing performance characteristics. This is a novel testing strategy based on the design of experiments (DOE) with specific application principles of Taguchi. In many experiments today, the difference between DOE and Taguchi methods mainly lies in their application approach by Roy et al. [23]. The Taguchi method aims to design a manufacturing process less susceptible to quality variation factors.

Design of origami-shaped energy absorption box

The box is designed based on the following formulas:

$$\Psi = \pi - 4arctan\left(\frac{l}{c}cos\frac{\theta}{2}\right) \quad (1)$$

$$\theta = arccos\left[\left(\sqrt{2}-1\right)\frac{c}{l}\right] \quad (2)$$

$$cos\frac{\theta}{2} = tan\left(\frac{\pi}{2N}\right)\frac{c}{l} \quad (3)$$

Geometric parameters are represented in Figure 7a, including folding width c, box width b, and height l, and there is a relationship between the dihedral angle θ and angle Ψ represented as follows.

From here, six different origami-shaped energy absorption boxes are designed based on the geometric parameters outlined in by Yuan et al. [7] with a series of origami-shaped energy absorption boxes with different geometric cross-sectional cuts, including square cross-section (A1, A2), rectangular (B4), triangle (C1), pentagon (C2), and hexagon (C3) cross-sections. While the cross-sectional shapes vary across these designs, the fundamental origami folding principle, governed by Equations 1–3 and the relationships between dihedral angles (θ) and angles (Ψ) as established by Yuan et al. [7], is consistently applied to each profile. Consequently, the distinct 'side surface shaping' observed for each type (A1, A2, B4, C1, C2, C3), as depicted in Figure 8, is not arbitrary but rather a direct adaptation of this core origami design principle to its specific cross-sectional geometry. This systematic approach ensures that the comparison of their crashworthiness performance remains valid and attributable to the variations in the base cross-sectional geometries. Below is the detailed table of geometric parameters of origami-shaped collision energy absorption boxes. The 3D geometries of the impact energy absorption chamber are shown after design based on the

Table 1. Geometric parameters of collision energy absorption boxes [7]

Type/form	N	a (mm)	b (mm)	c (mm)	l (mm)
A1	4	-	60	-	-
A2	4	-	60	30	60
B4	4	70	50	20	40
C1	3	-	80	14,35	40
C2	5	-	48	25,50	40
C3	6	-	40	30,92	40

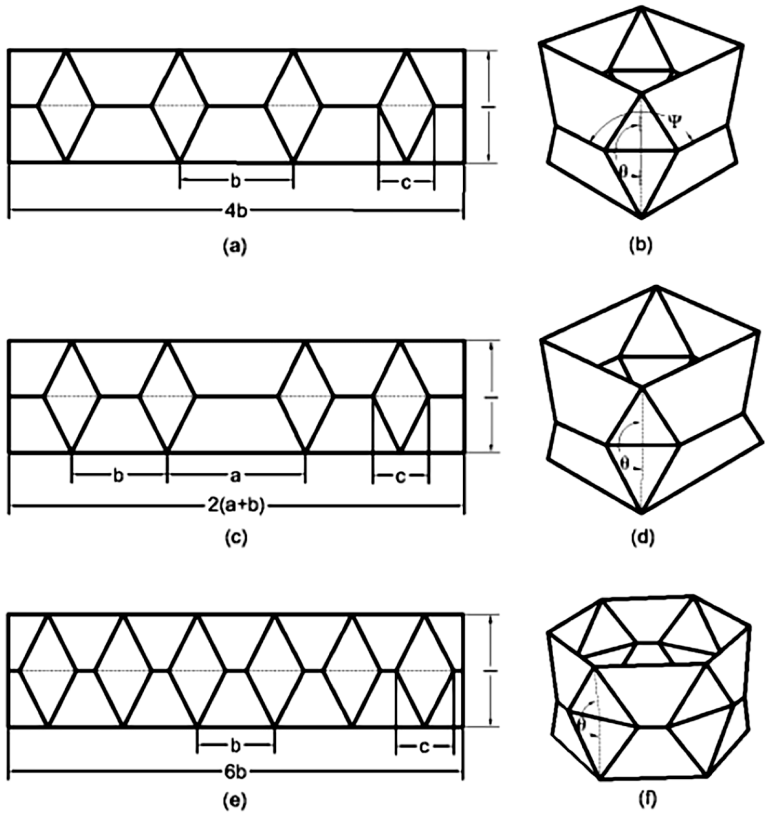

Figure 7. Shape of impact energy absorption box [7]

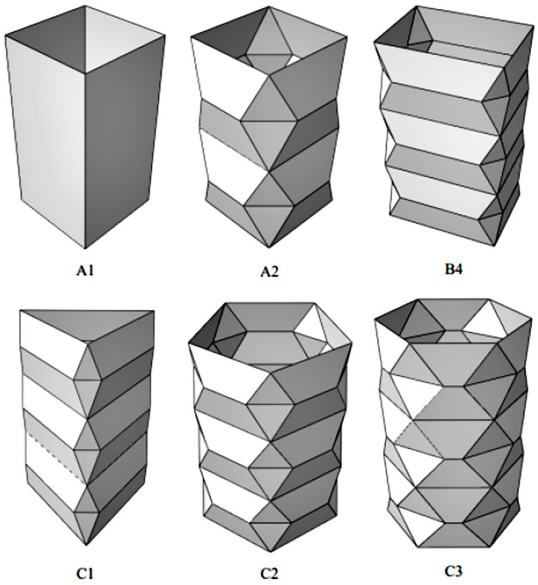

Figure 8. Specific shape of impact energy absorption box

Table 2. CFRP material parameters

Characteristic parameters	T300 fibers	Units
Density	1570.5	kg/m^3
Longitudinal elastic modulus	55.8	GPa
Transverse elastic modulus	55.8	GPa
Poisson's ratio	0.06	–
Shear modulus	3650	MPa
Longitudinal tensile strength	630	MPa
Transverse tensile strength	630	MPa
Longitudinal compressive strength	550	MPa
Transverse compressive strength	550	MPa
Shear strength	100	MPa
Longitudinal tensile fracture energy	45.8	kJ/m^2
Longitudinal compressive fracture energy	39.95	kJ/m^2
Transverse tensile fracture energy	45.8	kJ/m^2
Transverse compressive fracture energy	39.95	kJ/m^2

geometric parameters in Table 1 and the shape of the energy absorption chamber in Figure 7.

CFRP material model

Various types of carbon fiber materials are utilized in practical applications and in previous research. However, T300 fibers are chosen as the material model for this study due to their widespread use in the automotive industry owing to their high mechanical properties and reliability by Patruno et al. [25]. The carbon fiber T300 specifications are referenced from prior research by Chen et al. [26] and detailed in Table 2.

In this work, three geometric features of CFRP materials were considered to investigate their effect on the energy absorption capability of the structure. Specifically, these three parameters include the fiber orientation angle of the innermost layer ($\theta 1$), the fiber orientation angle of the outermost layer ($\theta 2$), and the thickness of the layer (t), as shown in Table 3. For convenience in subsequent research, the orientation angles of the inner layers ($\theta 1$) = -45°, the orientation angles of the outer layers ($\theta 2$) = -45°, and the thickness of a layer (t) = 0.1 mm are chosen as the basic geometric parameters of the material. The Taguchi method will systematically evaluate these parameter sets in the following section.

As shown in Figure 9, the laminate comprises a total of 13 layers, maintained constant throughout the study. This includes four inner and outer layers, five intermediate layers, and a central 0° layer oriented along the compression axis to enhance energy absorption and ensure pure compressive failure instead of torsional deformation.

Load modes

In research studies, researchers have shown interest in various types of load modes both in theoretical studies and practical cases. The following describes some common load modes, aiding in a better understanding of these load types: axial load; shear load; lateral load and bending load (Figure 1). Although various loading conditions have been investigated, most

Table 3. Geometric parameters of CFRP material

Parameter	Value		
	1	2	3
Innermost layer orientation angle (θ10)	-45	45	90
Outermost layer orientation angle (θ20)	-45	45	90
Thickness per layer (t_mm)	0,1	0,125	0,15

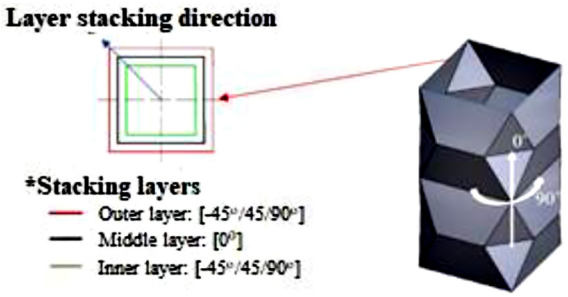

Figure 9. Overall shape and layer arrangement of the box

studies have focused on axial loading because it allows for accurate analysis and evaluation of a structure's energy absorption capabilities by several authors [28–30]. When a structure is subjected to axial loading, factors such as strength, elasticity, and stability are all examined and assessed. Previous studies have demonstrated that focusing on this loading condition yields crucial insights into stability and high energy absorption capabilities by Kumar et al. [31]. Therefore, axial loading was chosen as the loading condition in this study.

SIMULATION ANALYSIS OF MATERIAL PARAMETERS' INFLUENCE ON ENERGY ABSORPTION PERFORMANCE OF COLLISION ENERGY ABSORBERS

Simulation calculation

This study selects material parameters—inner layer orientation angle (θ1), outer layer orientation angle (θ2), and layer thickness (t)—as three control factors for Taguchi experimental design, with each element comprising three specified levels. Thus, an L9 (3^3) orthogonal array is constructed, indicating 9 experimental runs for 3 factors, each with 3 levels. This array will be referred to when using the Taguchi method, as mentioned above. For convenience in subsequent research sections, the set of parameters with inner layer orientation angle (θ_1) = -45°, outer layer orientation angle (θ_2) = -45°, and layer thickness (t) = 0.1 mm is chosen as the primary material geometry parameters. The geometric structure of the origami-shaped collision energy absorber box with various cross-sectional geometries, including square cross-sections (A1, A2), rectangular (B4), triangular (C1), pentagonal (C2), and hexagonal (C3) cross-sections, combined with the set of basic material geometric parameters, is provided for comparison and evaluation of SEA and PCF indices to determine the optimal structure. Subsequently, using this structure combined with the parameters in Table 1 in section Design of origami-shaped energy absorption box, SEA and PCF results of parameter sets used as input parameters for Taguchi are obtained. The entire process is simulated using ABAQUS software, and the simulation method will be presented as follows.

Simulation procedure of crash energy absorption box on ABAQUS

The simulation is conducted using the finite element method on ABAQUS. Model Figure 11 is designed in SOLIDWORKS software and imported into ABAQUS for computational simulation. The procedure for simulating collision energy absorption in the ABAQUS program is presented.

The CFRP material is defined by providing attribute data for the material from Table 2 into ABAQUS. Multiple failure criteria are employed to assess the failure of composite materials. The Hashin failure criteria provide relatively stable behavior and failure mode predictions. It can forecast initial failure and correlate with material

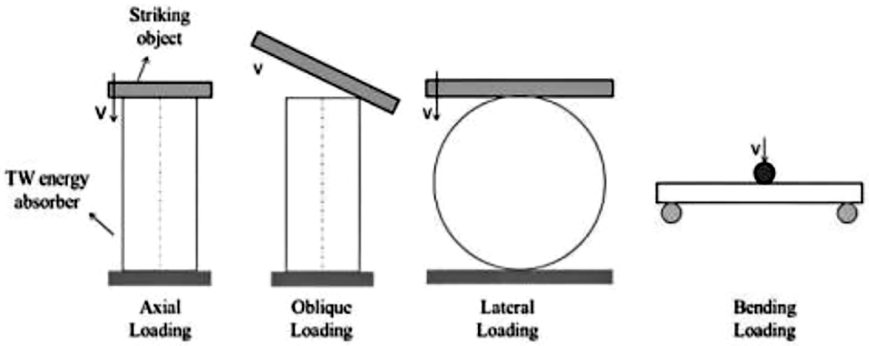

Figure 10. Load modes [27]

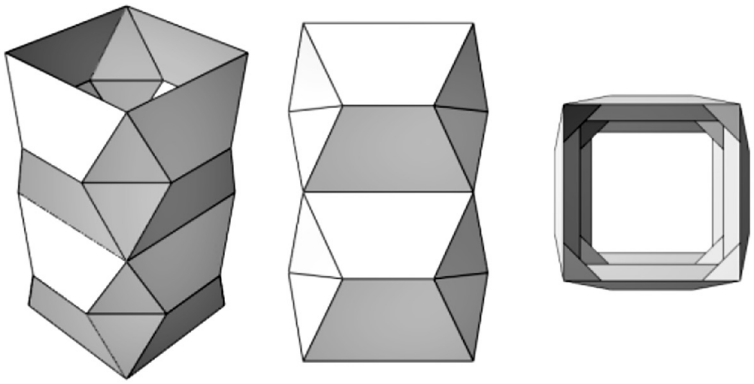

Figure 11. Three projections of the crash energy absorption box

failure criteria to delineate a failure process based on the fracture energy of various failure types [32]. The Hashin failure criteria are formulated as follows [33].

$$F_f^t = \left(\frac{\sigma_{11}}{X_t}\right)^2 + \alpha\left(\frac{\tau_{12}}{S_l}\right)^2 \quad \sigma_{11} \geq 0 \tag{4}$$

$$F_f^c = \left(\frac{\sigma_{11}}{X_t}\right)^2 \quad \sigma_{11} \leq 0 \tag{5}$$

$$F_m^t = \left(\frac{\sigma_{22}}{Y_t}\right)^2 + \left(\frac{\tau_{12}}{S_l}\right)^2 \quad \sigma_{22} \geq 0 \tag{6}$$

$$F_m^c = \left(\frac{\sigma_{22}}{2S_t}\right)^2 + \left[\left(\frac{Y_c}{2S_t}\right)^2 - 1\right]\frac{\sigma_{22}}{Y_c} + \left(\frac{\tau_{12}}{S_l}\right)^2 \quad \sigma_{22} \leq 0 \tag{7}$$

Boundary conditions

This model is subjected to two boundary conditions, detailed as follows. The box is placed between two parallel rigid panels. The upper rigid panel represents the compressing machine moving along the Y-axis direction, being compressed with a maximum displacement of 110 mm, as depicted in Figure 12. The lower rigid panel represents the fixture of the object of the compressing machine, constrained with 6 degrees of freedom, as shown in Figure 13.

Mesh division

The mesh module contains tools allowing us to create clusters and divide the mesh according to each box component. Various levels and types of meshes are available to meet the analysis requirements of the problem. Two rigid panels that do not deform are divided into a 10 mm mesh size to optimize the problem. The box is constructed using predominantly S4R shell elements for the mesh, augmented by triangular prism elements to mitigate excessive distortion [8]. To ensure mesh independence, a sensitivity analysis using 2 mm, 1 mm, and 0.5 mm sizes was performed on the C2 structure, showing negligible variation (<1% for SEA and PCF) between the 1 mm and 0.5 mm meshes. Therefore, a mesh size is 1mm, and

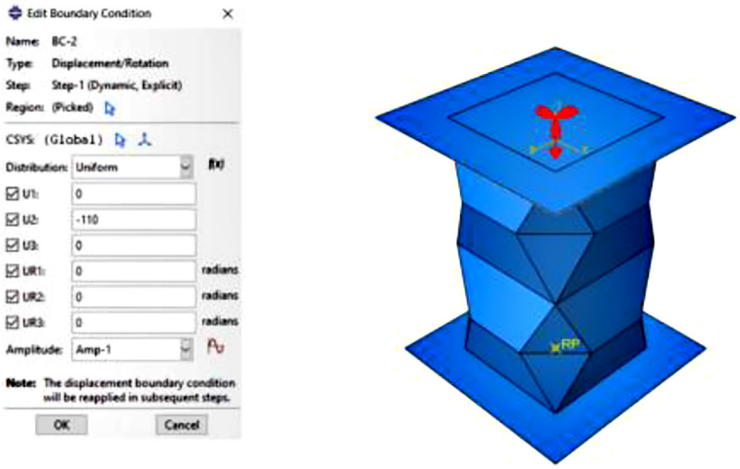

Figure 12. Implementation process of boundary condition 1

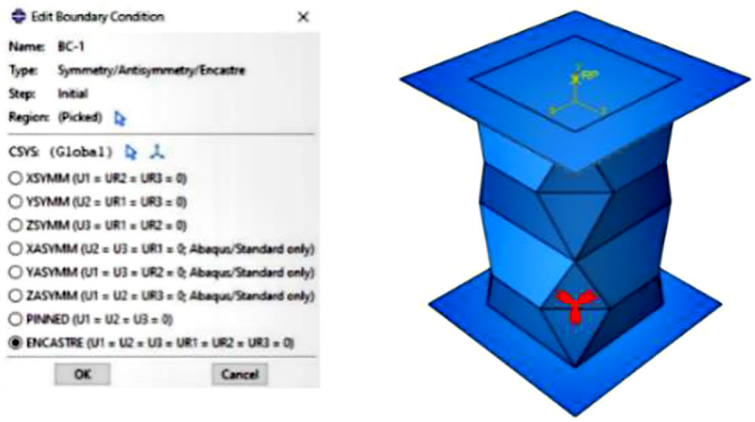

Figure 13. Implementation process of boundary condition 2

the total number of elements is 36029. Figure 14 shows the mesh after division.

Finally, for model validation, due to the lack of specific experimental data for the exact origami CFRP geometries studied, the numerical model's general behavior and failure modes were qualitatively compared against established experimental findings for similar composite crash absorbers in the literature [2, 10, 11]. The observed progressive failure (fiber fracture, matrix cracking, and delamination) and force-displacement trends were consistent with reported composite structures. Future work will include quantitative experimental validation.

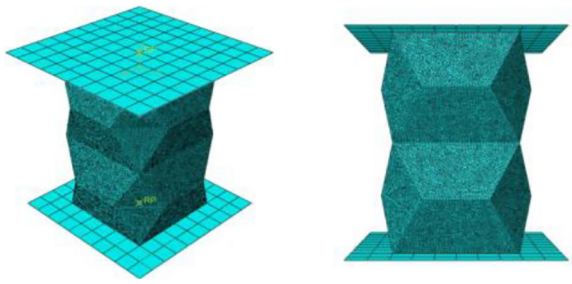

Figure 14. Grid division process of impact energy absorption box

RESULTS AND DISCUSSION

Comparison and evaluation of energy absorption box structures and materials in collision

Table 4 shows the aluminum material parameters that were referred to in previous studies. [34]. The force-displacement graph in Figure 15 vividly illustrates the fluctuations in force and displacement during the crushing process. The PCF of the energy-absorbing box constructed from CFRP material substantially exceeds that of the box made from aluminum material. However, due to the aluminum box's material characteristics, during the final crushing stage, when it reaches its maximum crush, indicating the loss of energy absorption capability, the crushing force increases abruptly. This event is anticipated to result in a decline in the energy absorption index (EA), hence leading to a decrease in the SEA index. Detailed calculations have been performed and compared through the table below to validate this issue accurately.

From Figure 16, it can be seen that the predictions made above are correct. The boxes' specific

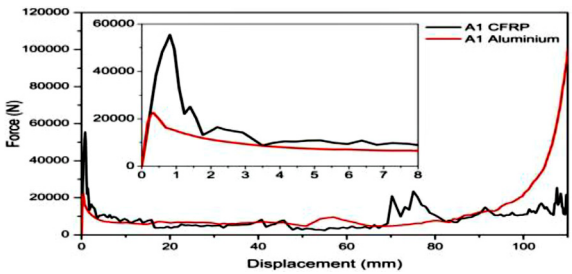

Figure 15. Force-displacement diagram

Table 4. Aluminum material parameters

Materials	E (GPa)	Y (GPa)	Poisson's ratio	ρ (kg/m^3)
Aluminium Alloy 6060-T5	69.5	243	0.33	2700

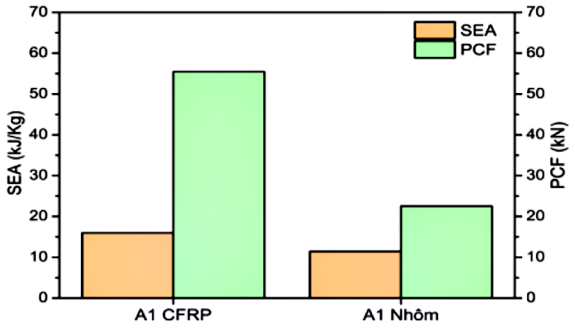

Figure 16. Comparison chart of SEA and PCF between CFRP and aluminum

SEA using CFRP and aluminum materials are 16 and 11.4 kJ/kg, respectively. From this, it can be seen that the box using CFRP material has a SEA 40% higher than that of aluminum. Despite having such superior SEA, CFRP material has a maximum PCF nearly 2.5 times higher than the box using aluminum material.

This observation indicates that the impact energy absorbing box using CFRP material possesses significantly higher SEA than aluminum material. However, as mentioned above, CFRP material has a very high PCF, so to overcome this, research on using alternative geometric models for impact energy-absorbing boxes will be conducted. The origami structure will be investigated and researched in impact energy-absorbing boxes.

Comparison of origami structures utilized in impact energy absorption boxes

This section analyzes five origami-shaped impact energy absorption boxes constructed from CFRP material, employing fundamental geometric characteristics with cross-sectional shapes of square, rectangle, triangle, pentagon, and hexagon, as depicted in Figure 8.

The graph in Figure 17 clearly illustrates the force and displacement values at each stage of the crushing operation. In the preliminary phase of the crushing process, structure C3 demonstrates the highest PCF crushing force of 37, succeeded by B4, A2, C1, and C2, which exhibit the lowest PCF values. This signifies substantial variations in the maximum of PCF across buildings with diverse cross-sectional geometries. Simultaneously, these cross-sectional geometries will influence the values of the specific energy absorption index (SEA). The subsequent section will address These two issues more precisely and in detail. A substantial link exists between the PCF and the SEA index of origami structures utilizing CFRP materials. Concerning PCF, the design aim of energy absorption structures is to mitigate the impact of accidents on vehicle occupants by reducing this force to enhance passenger safety. However, reducing PCF is often associated with decreasing SEA, as discussed in studies using metallic materials [35, 36], and interestingly, this is also observed in CFRP materials. Therefore, selecting a structure that appropriately balances PCF and SEA values will provide good energy absorption performance.

Figure 18 graphically represents the SEA index of structures A2, C1, and C2, with SEA thresholds fluctuating around 15 kJ/kg, while B4 and C3 exhibit significantly superior values, at 20.66 and 20.01 kJ/kg, respectively. However, structure B4 demonstrates a considerably higher PCF, approximately 43.1 kN, surpassing the other structures by 1.3 to 1.7 times, and structure C3 records the highest PCF of 54.6 kN, exceeding the others by 1.7 to 2.1 times. Consequently, neither is selected as a suitable structure for investigating geometric parameter effects. Furthermore, structure

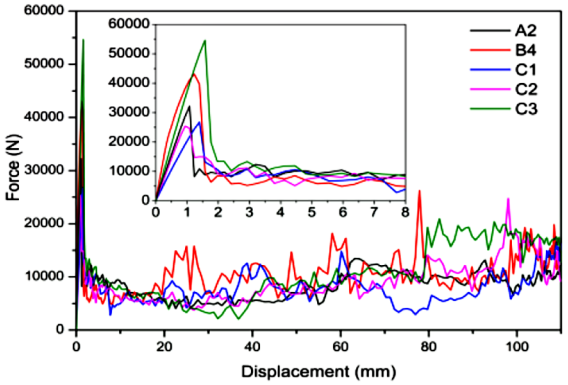

Figure 17. Force-displacement diagram among structures

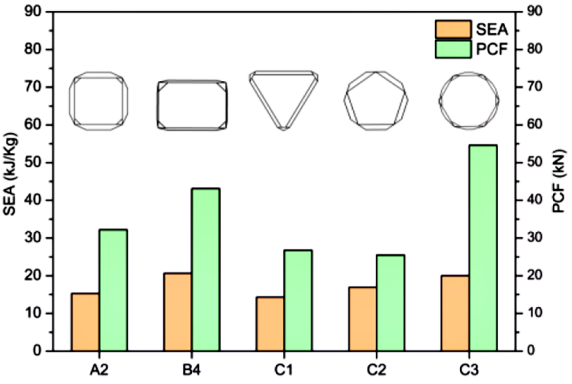

Figure 18. Comparison chart of SEA and PCF

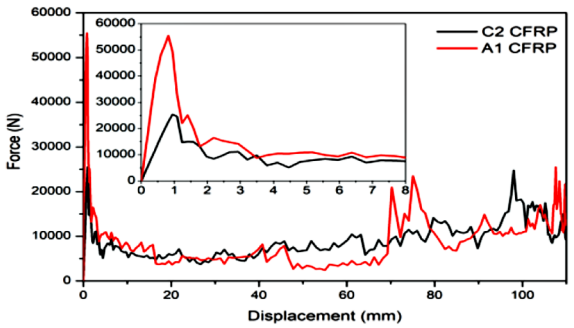

Figure 19. Force-displacement diagram of structure A1 – C2

C1 possesses relatively low PCF, but its energy absorption efficiency is also the lowest, rendering it unsuitable for material parameter influence studies. Considering the remaining structures, A2 and C2, with similar SEA values of 15.28 and 16.9 kJ/kg, respectively, structure A2 exhibits a significantly higher PCF of 32.2 kN compared to C2's 25.5 kN. Thus, structure C2 is chosen as the optimal structure for studying the effects of CFRP material parameters on its performance.

Based on the obtained SEA and PCF results, the following observations are drawn – with the same set of composite material parameters, structures C1 and C2 have the smallest PCF, which is advantageous for collision energy absorption box design. Other structures such as A2, B4, and C3 demonstrate elevated SEA values, although also possess considerably bigger PCF in comparison to the first two. Given that the SEA of structure C2 exceeds that of C1, its PCF is around 5% lower than that of C1, significantly outperforming the other structures; thus, structure C2 is selected for examining the influence of CFRP material characteristics on its energy absorption capabilities.

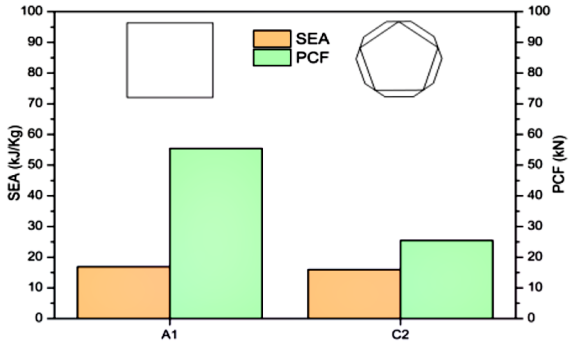

Figure 20. Comparison chart of SEA and PCF

Comparison of origami-shaped CFRP energy absorption boxes with square-shaped CFRP energy absorption boxes

The origami-shaped CFRP energy absorption box structure C2 was selected as the optimal structure for subsequent work. Next, details regarding evaluating the outstanding features of origami-shaped energy absorption boxes compared to square shapes will be presented by comparing a traditional square tube A1 and an origami-shaped energy absorption box C2 [26]. Both structures utilize the same material, CFRP, with basic geometric parameters to compare and evaluate geometric structures. Looking at Figure 19, it can be observed that the force-displacement diagram of the traditional square-shaped energy absorption box structure A1 has a much higher maximum PCF compared to the structure of energy absorption box C2. While structure A1 exhibits a much higher maximum PCF, the area under the force-displacement curve for structure C2 is marginally larger, indicating a slightly higher total energy absorption capacity despite its lower peak force. This contributes to C2's improved SEA value, even though its peak force is significantly lower. The origami-shaped energy absorption box explains that this C2 utilizes an origami structure. Previous research has demonstrated that origami structures help reduce maximum PCF and increase SEA.

Based on Figure 20, the following observations can be made: with the same set of composite material parameters but different geometric structures, the traditional square box structure A1 has a significantly higher PCF of 55.4 kN compared to the energy-absorbing origami structure C2 and nearly 118% higher than structure C2. Meanwhile, the SEA of structures A1 and C2 are 16 and 16.9 kJ/kg, respectively. While the increase in SEA of structure C2 compared to structure A1 is a modest 5%, the simultaneous and substantial 118% reduction in PCF is critical. This combined benefit signifies that the origami structure C2 offers a significantly more optimal performance profile for collision energy absorption compared to the square box A1, enhancing both energy absorption efficiency and passenger safety. This has also been demonstrated in previous research using metal materials [26]. Therefore, an origami-shaped structure is more optimal than a conventional square box structure.

These investigations indicate that the integration of CFRP material with origami geometry is

the most effective option for collision energy-absorbing boxes. CFRP material exhibits a 40% more specific energy absorption (SEA) than traditional aluminum, while the origami-shaped collision energy-absorbing box C2 can diminish the PCF by more than twofold in comparison to the typical square tube construction. The results will provide a systematic investigation of the impact of CFRP material characteristics on the energy absorption performance of the origami structure, which will be detailed in the subsequent section.

Design of CFRP material parameter set

Application of Taguchi method for CFRP material parameter set design

The primary process of Taguchi is encapsulated as follows:

- Step 1: Taguchi experimental design

Developing Taguchi orthogonal arrays (OAs), wherein control factors form the inner array and noise factors comprise the outside array. Conducting experiments for each sample and obtaining responses.

This study selected three control factors: the orientation angles of inner layers ($\theta 1$), the orientation angles of outer layers ($\theta 2$), and the thickness of a layer (t), each with three specified levels as detailed in Table 3. An L9 (3^3) orthogonal array was subsequently created to create the inner array. In this study, SEA and PCF were regarded as replies. Table 5 displays the constructed OA table for the Taguchi experimental design, specifically formulated to assess the primary impacts of design variables and their interactions with responses.

After utilizing the geometric parameters from Table 5 for the CFRP-based structure C2 as input parameters for ABAQUS, the program will simulate and yield the energy absorption index EA results. Subsequently, the index SEA and maximum PCF will be computed according to the formulas in section 2. The calculated results of SEA and PCF from Table 6 will be utilized as input parameters for Taguchi.

- Step 2: Signal-to-noise ratio (S/N Ratio)

After completing the Taguchi experimental design and calculating the response data for each factor level, the signal-to-noise ratio (SNR) is employed to quantify the mean value of a process in relation to its variation, as well as to evaluate the response performance concerning the relevant characteristics. The SNR for a response exhibiting the larger-the-better (LTB) characteristic can be determined using Equation 8, whereas the SNR for a response exhibiting the smaller-the-better (STB) characteristic can be calculated using Equation 9.

$$SN\ R_{ij} = -10\log_{10}\left(\frac{1}{10}\sum_{k=1}^{n}\frac{1}{y^2{}_{ijk}}\right) \quad (8)$$

$$SN\ R_{ij} = -10\log_{10}\left(\frac{1}{10}\sum_{i=1}^{n}y^2{}_{ijk}\right) \quad (9)$$

SN Rij denotes the signal-to-noise ratio (SNR) for the j_{th} response of the i_{th} experiment, whereas represents the experimental outcome for the j_{th} response of the i_{th} experiment at the k_{th} measurement, and n signifies the total number of measurements per experiment. This study selected two conflicting responses, SEA and PCF, for measurement and evaluation. As known, an enormous SEA (LTB) is preferable to enhance overall energy absorption capability, whereas a smaller PCF (STB) is preferable to control the severity of the load. Therefore, Equations 8 and 9 are applied to SEA and PCF to calculate the corresponding SNR.

Results

The experimental findings derived from the Taguchi orthogonal array are provided in this paragraph. The statistical software Minitab executed all experimental design procedures and Taguchi analyses. The Anderson-Darling test was utilized

Table 5. Orthogonal array L9(3^3) for current research

No.	Inner layer orientation angle (θ_1 [°])	Outer layer orientation angle (θ_2 [°])	Thickness of each layer (t [mm])
1	-45	-45	0.100
2	-45	45	0.125
3	-45	90	0.150
4	45	-45	0.125
5	45	45	0.150
6	45	90	0.100
7	90	-45	0.150

Table 6. Input parameters for taguchi analysis

No.	Mass	EA	SEA	PCF
	kg	kJ	(kJ/kg)	kN
1	0.0584	0.98783	16.91	25.47
2	0.073	1.2372	17.94	38.9
3	0.0876	1.59633	18.22	47.23
4	0.073	1.1354	15.55	38.38
5	0.0876	1.48625	16.96	49.7
6	0.0584	0.99402	17	26.53
7	0.0876	1.52575	17.4	47.48
8	0.0584	1.01129	17.31	26.3
9	0.073	1.31435	18	33.03

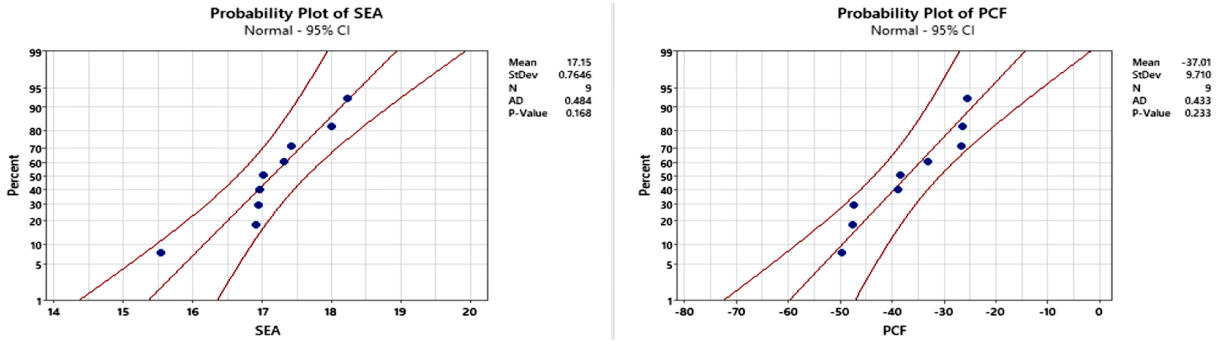

Figure 21. Probability chart

Table 7. Response table for s/n ratio of sea

No.	Inner layer orientation angle (θ_1[°])	Outer layer orientation angle (θ_2[°])	Thickness of each layer (t [mm])
1	24.79	24.41	24.65
2	24.35	24.65	24.51
3	24.90	24.98	24.87
Delta	0.55	0.57	0.37
Rank	2	1	3

to validate the normalcy assumption, a commonly accepted and rigorous technique for identifying departures from normality. Figure 21 demonstrates that the statistical values of the Anderson-Darling test are minimal, and all p-values exceed 0.05, so indicating that the experimental data conforms to a normal distribution. Figure 21 illustrates that the experimental data for all responses (SEA, PCF, and overall response) closely corresponds with the fitted line. Consequently, analysis and assessments may be conducted on this response data. The assumption of normality is essential for performing some statistical tests in Taguchi analysis. The normality assumption serves as a reliable indicator of the absence of outliers in the data [37].

Analyzing the influence of parameters on SEA and PCF based on Taguchi method results

Figure 22 illustrates the principal effects of material design factors (θ_1, θ_2, and t) on SEA and PCF. The main effects plots (Figure 22) illustrate the influence of each parameter at its different levels on the S/N ratio. For all performance characteristics (larger-the-better for SEA, smaller-the-better for PCF), a higher S/N ratio generally indicates better performance and less variability. However, the calculation of the S/N ratio is tailored to the objective: for 'larger-the-better' characteristics (SEA), higher S/N implies a greater response value, while for 'Smaller-the-Better'

Table 8. Response table for pcf s/n ratio

No.	Inner layer orientation angle (θ_1 [°])	Outer layer orientation angle (θ_2 [°])	Thickness of each layer (t [mm])
1	-31.14	-31.11	-28.33
2	-31.36	-31.38	-31.29
3	-30.77	-30.78	-33.65
Delta	0.59	0.60	5.32
Rank	3	2	1

characteristics (PCF), higher S/N implies a smaller response value. The optimal level for each parameter is identified by the level that yields the highest S/N ratio for its respective objective. The "Delta" value in the response tables (Tables 7 and 8) indicates the magnitude of each factor's effect, with a larger delta implying a more significant influence.

As illustrated in Figure 22(a) and supported by Table 7 (No.1 for θ_2), the orientation angle of the outermost layer (θ_2) is identified as the most significant influencing factor on SEA, followed by the orientation angle of the innermost layer (θ_1) and the thickness of each layer (t). The chart also illustrates a notable trend where an increase in the outer angle leads to an increase in the S/N ratio of SEA. Furthermore, based on the primary effects on the S/N ratio of SEA, the optimal structure is achieved at $\theta_1(3)$, $\theta_2(3)$, and $t(3)$. In other words, the SEA response value can be maximized when inner and outer angle values (θ_1 and θ_2) are 90° and the thickness of each layer (t) is 0.15 mm.

Additionally, the results of the material parameter influences on the PCF of the structure, as presented in Figure 22b and Table 8 (No. 1 for t), indicate that the thickness of each layer has the most significant impact on the PCF value. While the inner and outer angles play less dominant but comparable roles, the signal-to-noise ratio of PCF diminishes with an increase in the thickness of each layer. The optimal levels of material parameters for PCF, based on their principal effects on the S/N ratio, are attained at $\theta_1(3)$, $\theta_2(3)$, and $t(1)$. The optimal PCF response value is attained when the inner and outer angles (θ_1 and θ_2) are 90° and the thickness of each layer (t) is 0.1 mm. Based on the observed results, the influence of CFRP material parameters on SEA and PCF, which are inherently contrasting objectives, are not uniform.

Validation of optimal parameter set using Taguchi method

To validate the precision of the Taguchi approach, a pair of parameters optimizing two indices, SEA and PCF, will be selected. The parameters for these optimal values are listed

Table 9. Optimization parameters set for sea and pcf

No.	Inner layer orientation angle (θ_1 [°])	Outer layer orientation angle (θ_2 [°])	Thickness of each layer (t [mm])
SEA	90	90	0.15
PCF	90	90	0.1

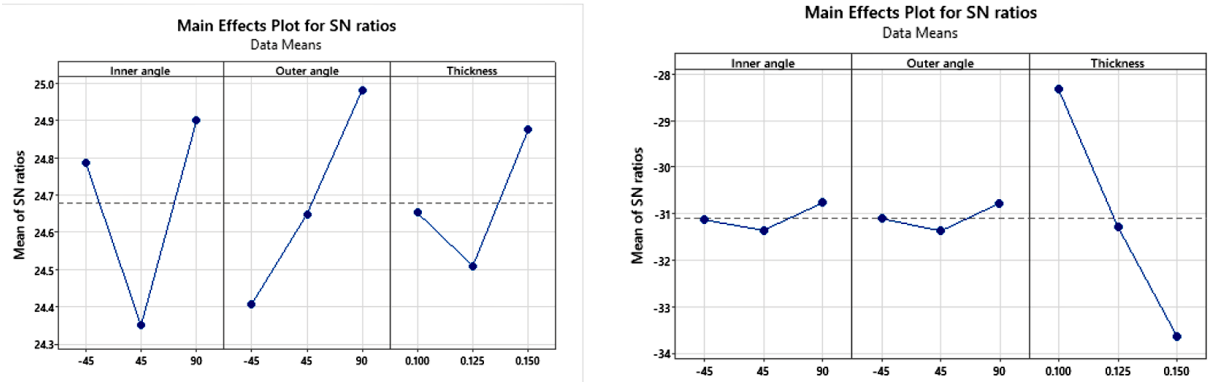

Figure 22. Principal parameter influence chart of material parameters on SEA/PCF S/N ratio

in Table 9. In this section, the pentagonal origami energy-absorbing box C2, made of 47 CFRP material with optimized SEA and PCF parameters, will be compared with the conventional square energy-absorbing box A1, made of commonly used aluminum material, and the pentagonal origami energy-absorbing box C2, made of CFRP material with pre-studied basic parameters.

As illustrated in Figure 23, significant differences in force and displacement throughout the crushing process of all three structures are evident. The PCF force of the energy-absorbing box using CFRP material with optimized SEA parameters is twice as large as the traditional square box A1 using aluminum material and the pentagon box C2 using CFRP material with basic parameters. Variations in PCF force often correlate with fluctuations in the SEA index. Furthermore, Figure 23 demonstrates that this structure's energy absorption area (EA) is considerably higher than the other two structures. Therefore, it is predicted that the SEA of the energy-absorbing box using CFRP material with optimized SEA parameters will meet expectations. Further calculations and comparisons are conducted in the subsequent section to test this hypothesis robustly.

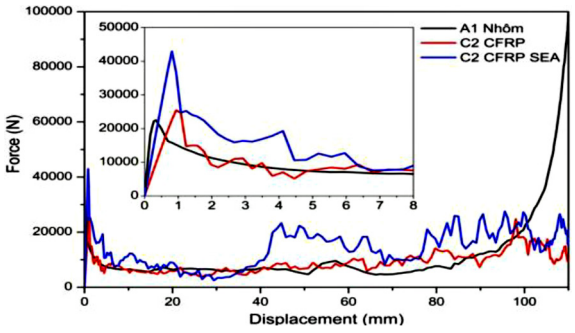

Figure 23. Force-displacement diagram

Through the chart in Figure 24, it is observed that the energy-absorbing box using CFRP material with optimized SEA parameters provides a better SEA index compared to the traditional square box A1 using aluminum material and the pentagon box C2 using CFRP material with essential parameters of 55% and 11%, respectively, as initially predicted. Hence, the Taguchi optimization method accurately predicted the optimized parameters for the SEA index. To further validate the accuracy of this method, a study on PCF optimization will be discussed in the subsequent section.

Optimization of PCF

Referring to Figure 25, the structure with the lowest PCF is the traditional square-shaped crash energy absorption box A1 made of aluminum, followed by the pentagon-shaped crash energy absorption box C2 made of CFRP with optimized PCF parameters and the pentagon-shaped crash energy absorption box C2 made of CFRP with basic parameters. Although not the structure with the highest PCF, the pentagon-shaped crash energy absorption box C2 made of CFRP with optimized PCF parameters has improved by approximately 1.1 kN compared to the structure of the pentagon-shaped crash energy absorption box C2 made of CFRP with basic parameters. Therefore, this structure has demonstrated that the Taguchi method has optimized the precise parameters to reduce PCF crushing force compared to the structure using basic parameters.

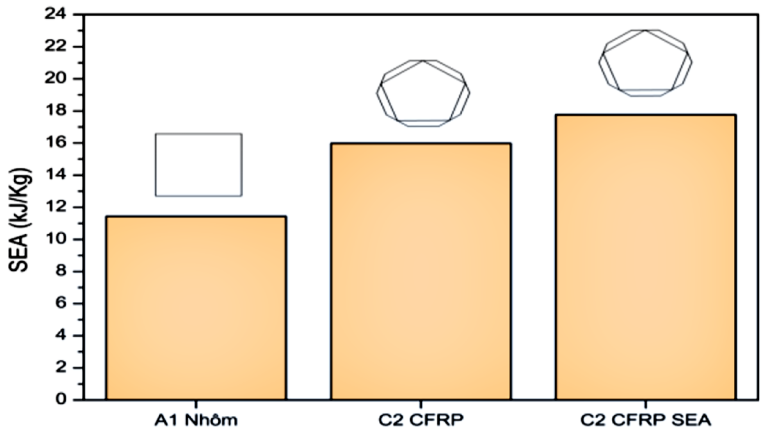

Figure 24. Comparative SEA chart

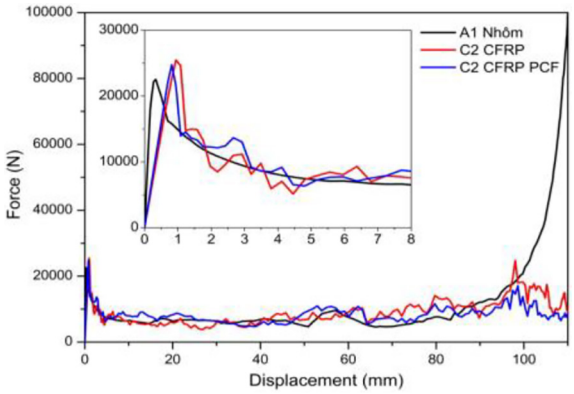

Figure 25. Force displacement graph

Destructive behavior

The axial crushing behavior of thin-walled, ductile metallic alloy components with certain shapes has been thoroughly examined for their energy absorption potential. This phenomenon is indicative of how metals like aluminum absorb substantial energy through their intrinsic plastic deformation capabilities and progressive folding during the crushing phase. The traditional square-shaped impact energy absorption box A1 made of aluminum material has been proposed to study this behavior.

The crushing reaction in the current study is divided into initial and secondary stages. The initial stage occurs before reaching the collapse, i.e., before the occurrence of maximum crushing force when the box has not yet deformed because it can still resist the gradually increasing crushing force. However, the box cannot maintain this state for long as the crushing force increases significantly; the box then transitions to the secondary stage. In this stage, the box undergoes extensive axial loading, leading to bending in the side walls and the formation of folds on the sidewalls, corresponding to the variation in the displacement force curve. The interaction between adjacent sidewalls and the contact of the folds create the formation of subsequent folds with a constant wavelength along the remaining length of the box, allowing the box to absorb impact energy. Details of the changes in the A1 impact energy absorption box during crushing will be illustrated in Figure 26.

Figure 26 shows that, from the elastic phase to the beginning of the failure phase, structure A1, using aluminum material, exhibits relatively minimal displacement. This indicates that the impact force is evenly distributed during a direct collision, thereby reducing the force exerted on passengers and enhancing passenger safety. When folding attains around 93 mm, the creases generated from the original folding process interlock, rendering further compression unfeasible. The crash energy absorber underwent complete deformation as its energy absorption capacity was fully depleted. Conversely, Figure 27 illustrates that the origami-shaped crash energy absorption box C2, made of CFRP composite material, has a more extended energy absorption phase than the A1 crash energy absorption box using aluminum – up to 110 mm with no signs of stopping. This is due to the distinctive failure mode of CFRP material compared to aluminum. Unlike the plastic deformation observed in metals, CFRP material, when compressed, exhibits brittle failure mechanisms such as progressive fracturing, delamination, fiber breakage, and matrix cracking. These progressive damage modes gradually crush the material, absorbing energy throughout this continuous degradation process until there is no longer any structural integrity. Therefore, instead of forming compact folds through plastic

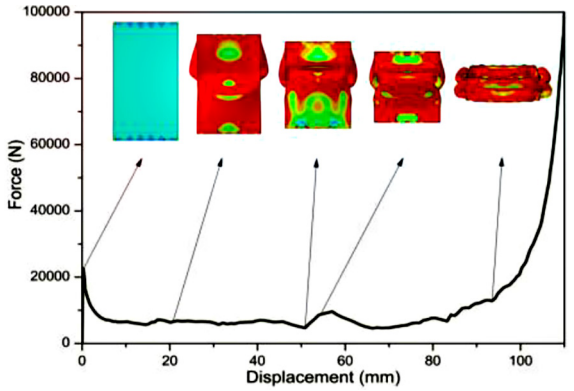

Figure 26. Deformation behavior of structure A1 using aluminum material

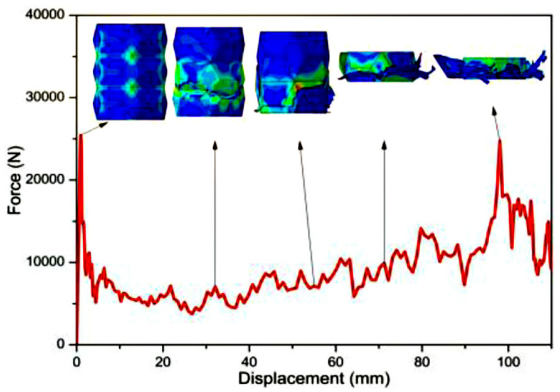

Figure 27. Structural destruction behavior of C2 utilizing basic material parameters

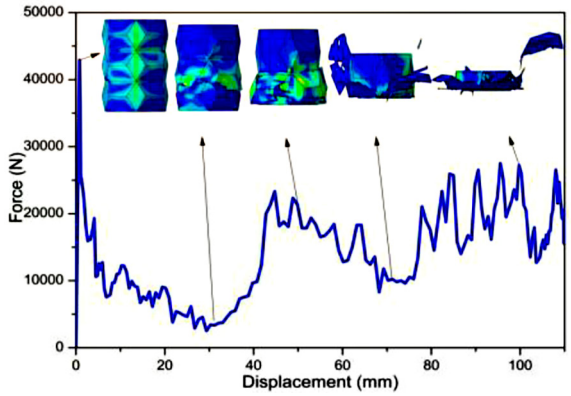

Figure 28. Structural destruction behavior of C2 structure using optimized SEA parameters

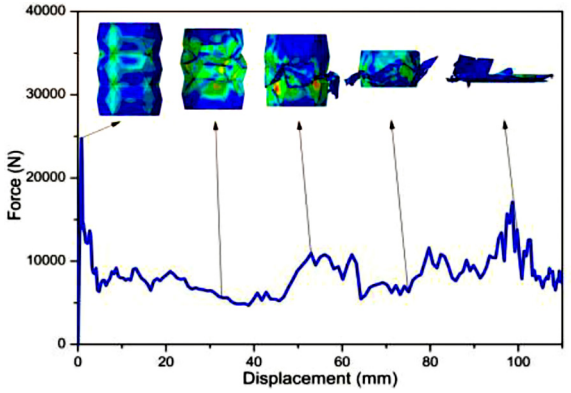

Figure 29. Structural destruction behavior of C2 structure using optimized PCF parameters

deformation like aluminum, CFRP continues to absorb energy through these progressive damage modes, which prevents a sudden increase in crushing force due to material stacking and allows for a more stable and prolonged energy absorption phase.

Figure 28 illustrates that, despite a substantial enhancement in the SEA value of the structure, its initial force is greater than that of both the original structure and the optimized PCF structure depicted in Figure 29, and vice versa. The reason is that improving SEA in the structure to a thinner one often increases the maximum crush force (PCF) [35, 36]. Additionally, since the structure is selected based on the reflection of parameter influence on the structure's performance through the Taguchi method, PCF and SEA parameters have yet to be optimized simultaneously. This opens up a future research direction on using multi-objective optimization methods to achieve an optimal structure to minimize PCF maximum crush force and improve SEA values simultaneously. Furthermore, the force-displacement graphs obtained from these analyzed structures all demonstrate the destruction behavior of CFRP materials, indicating an elongated compelling crash energy absorption journey due to the absence of material layer stacking phenomenon, as observed in metallic materials in Figure 25.

CONCLUSIONS

In conclusion, the origami-shaped energy-absorbing box constructed from CFRP material has been designed and implemented utilizing the Taguchi technique to assess the impact of material parameters on the energy-absorbing efficacy of the collision energy-absorbing box. The results acquired are as follows:

1. For equivalent weight and dimensions, CFRP material exhibits a significantly superior specific energy absorption capacity, exceeding that of an aluminum box by up to 40%. While CFRP inherently presents a higher peak crushing force in unoptimized forms, the strategic integration of origami geometry is crucial in mitigating this characteristic.
2. Among the investigated CFRP origami structures, the C2 structure (pentagon cross-section) consistently demonstrated superior SEA and markedly lower PCF values compared to the other four designs (A1, A2, C1, C3). This highlights the C2 profile as an optimal geometric configuration for energy absorption.
3. The optimized origami-shaped collision energy-absorbing box C2 using CFRP material significantly outperforms conventional square aluminum tube structures. Specifically, the C2 structure achieves improved SEA by 5% (over the baseline square aluminum tube) and, critically, reduces the PCF by approximately 118% (over twofold) compared to the conventional square aluminum tube. This conclusively demonstrates that the carefully designed origami structure effectively overcomes the inherent challenge of CFRP's relatively high PCF, transforming it into a highly efficient energy absorber.

Practical implications and shaping guidance: the integration of CFRP with optimized origami geometries, particularly the pentagonal C2 profile, represents a highly promising approach for shaping energy absorbers to achieve superior crashworthiness. This research provides clear

guidance: to maximize SEA while simultaneously minimizing PCF, absorbers should be designed with specific origami features, such as the C2's pentagonal cross-section, which promote stable, progressive crushing and controlled brittle fracture in CFRP materials. These findings offer valuable insights for the lightweight design of future automotive and aerospace components, promoting both enhanced safety and fuel efficiency.

The application of the Taguchi method successfully identified an optimal CFRP material parameter set for maximizing SEA and minimizing PCF individually, demonstrating the accuracy of this parameter set. However, these parameters were selected based on their independent influence. Future research should focus on using multi-objective optimization methods to achieve an optimal structure that simultaneously minimizes PCF and maximizes SEA, further enhancing the design of crash energy absorption boxes.

REFERENCES

1. Hussain, N Nasir, Srinivasa Prakash Regalla, and Yendluri V Daseswara Rao. Comparative study of trigger configuration for enhancement of crashworthiness of automobile crash box subjected to axial impact loading. Procedia Engineering 173 (2017): 1390–98. https://doi.org/10.1016/j.proeng.2016.12.198
2. Kadarno, P, Koronka Putukala, K, Purbolaksono, J, Turangga Bayu, A, Buys, YF, Barrinaya, MA and Kuang KC. Crashworthiness analysis of Cfrp crash box by finite element method. Paper presented at the Multimedia University Engineering Conference (MECON 2022), 2022. 10.2991/978-94-6463-082-4_21.
3. Pawlowski, M, Yigit, E and Meywerk, M. Finite element simulations of high-frequency crash signals for robust crash discrimination. Proceedings of the Institution of Mechanical Engineers, Part D: Journal of Automobile Engineering 2015; 229(13): 1762–73.
4. Ma, J, and You, Z. Energy absorption of thin-walled square tubes with a prefolded origami pattern—part I: Geometry and numerical simulation. Journal of applied mechanics 2014; 81(1): 011003.
5. Hou, D, Chen, Y, Ma, J and You, Z. Axial Crushing of Thin-Walled Tubes With Kite-Shape Pattern. ASME 2015 International Design Engineering Technical Conferences and Computers and Information in Engineering Conference, 2015: Paper No: DETC2015-46671. https://doi.org/10.1115/DETC2015-46671
6. Wang, B, and Zhou, C. The imperfection-sensitivity of origami crash boxes. International Journal of Mechanical Sciences 2017; 121: 58–66.
7. Yuan, L, Shi, H, Ma, J and You, Z. Quasi-static impact of origami crash boxes with various profiles. Thin-Walled Structures 2019; 141: 435–46.
8. Ma, J, and You, Z. The origami crash box. Origami 2011; 5(587): 277–290.
9. [9] Li, C, Li, X, Li, S, and Ma, S. Origami pattern tube for vehicle crash box. 2013.
10. Sun, G, Li, S, Li, G and Li, Q. On crashing behaviors of Aluminium/Cfrp tubes subjected to axial and oblique loading: an experimental study. Composites Part B: Engineering 2018; 145: 47–56.
11. Zhu, G, Sun G, Yu H, Li S, and Li Q. Energy absorption of metal, composite and metal/composite hybrid structures under oblique crushing loading. International Journal of Mechanical Sciences 2018; 135: 458–83.
12. Sun, G, Li, S, Liu, Q, Li, G and Li, Q. Experimental study on crashworthiness of empty/aluminum foam/honeycomb-filled Cfrp tubes. Composite Structures 2016; 152: 969–93.
13. Liu, Y, Zwingmann, B and Schlaich, M. Carbon fiber reinforced polymer for cable structures—a review. Polymers 2015; 7(10): 2078–99.
14. Hussain, NN, Regalla SP, and Rao, YVD. Study on influence of notch triggers on absorption of energy for composite automobile crash box under impact loads. Materials Today: Proceedings 2021; 38: 3220–31.
15. Wang, G, Zhang, Y, Zheng, Z, Chen, H and Yu J. Crashworthiness design and impact tests of aluminum foam-filled crash boxes. Thin-Walled Structures 2022; 180: 109937.
16. Tan, H, He, Z, Li, E, Cheng, A, Chen, T, Tan, X, Li, Q and Xu, B. Crashworthiness design and multi-objective optimization of a novel auxetic hierarchical honeycomb crash box. Structural and Multidisciplinary Optimization 2021; 64(4): 2009–24.
17. Võ, NC. Tính Kết Cấu Theo Phương Pháp Phần Tử Hữu Hạn. 2005.
18. Khalkhali, A, Masoumi, A, Darvizeh, A, Jafari, M and Shiri, A. Experimental and numerical investigation into the quasi-static crushing behaviour of the s-shape square tubes. Journal of Mechanics 2011; 27(4): 585–96.
19. Kim, HC, Shin, DK and Lee JJ. Characteristics of aluminum/Cfrp short square hollow section beam under transverse quasi-static loading. Composites Part B: Engineering 2013; 51345–58.
20. Wang, H, Hu, W and Zhao F. Numerical simulation of quasi-static compression on a complex rubber foam. Acta Mechanica Solida Sinica 2017; 30(3): 285–90.
21. Quanjin, M, Salim, MSA, Rejab, MRM, Bernhardi, O-E, and Nasution AY. Quasi-static crushing response of square hybrid carbon/aramid tube for automotive crash box application. Materials Today:

Proceedings 2020; 27: 683–90.

22. Rabiee, Ali. Lightweight design of multi-stitched composite crash absorbers to improve specific energy absorption capability under quasi-static and impact loading. 2018.
23. Roy, RK. Design of Experiments Using the Taguchi Approach: 16 Steps to Product and Process Improvement. John Wiley & Sons, 2001.
24. Shi, M, Ma, J, Chen, Y and You Z. Energy absorption of origami crash box: Numerical simulation and theoretical analysis. ASME 2018 International Design Engineering Technical Conferences and Computers and Information in Engineering Conference, (2018): Paper No: DETC2018-86261. https://doi.org/10.1115/DETC2018-86261
25. Patruno, L. Design of an origami shaped composite structure with application to a race car crash absorber. Politecnico di Torino, 2023.
26. Chen, Y, Ye, L and Fu K. Progressive failure of Cfrp tubes reinforced with composite sandwich panels: numerical analysis and energy absorption. Composite Structures 2021; 263: 113674.
27. Muchhala, D, Pandey A, Raj R, Sahu SK, Srivastava SK, and Mondal DP. Crashworthiness performance of foam filled composite tubular structures. In thin-walled composite protective structures for crashworthiness applications: Recent Advances and Future Developments, 25–40: Springer, 2023.
28. Santosa, S, and Tomasz Wierzbicki. Crash behavior of box columns filled with aluminum honeycomb or foam. Computers & Structures. 1998; 68(4): 343–67.
29. Ghasemnejad, H, Hadavinia, H, Marchant, D, and Aboutorabi, A. Energy absorption of thin-walled corrugated crash box in axial crushing. SDHM Structural Durability and Health Monitoring 2008; 4(1).
30. Choiron, MA, Happy, HK, Purnowidodo, A and Rivai A. Deformation Pattern and Energy Absorption Analysis on Initial Fold Crash Box by Oblique Crash Test. Paper presented at the IOP Conference Series: Materials Science and Engineering, 2019.
31. Kumar, AP, Dirgantara, T and Rangappa, SM. Thin-walled composite protective structures for crashworthiness applications: Recent advances and future developments. Springer, 2023.
32. Zhu, X, Chen, A, Huang, Z, Chen, Z, Lin, Y, and Li, Y. Quasi-static compression response of the origami thin-walled structure. Thin-Walled Structures. 2023; 183: 110376. https://doi.org/10.1016/j.tws.2022.110376
33. Jahani, M, Beheshti, H and Heidari-Rarani, M. Effects of geometry, triggering and foam-filling on crashworthiness behaviour of a cylindrical composite crash box. International Journal of Automotive and Mechanical Engineering 2019; 16(2): 6568–87.
34. Azizol, MNFB. The Study of Energy Absorption Capability with Different Crash Box Construction.
35. Yang, S, and Chang Q. Multiobjective optimization for empty and foam-filled square columns under oblique impact loading. International Journal of Impact Engineering 2013; 54: 177–91.
36. Cetin, E, Baykasoğlu, A, Erdin, ME and Baykasoğlu, C. Experimental investigation of the axial crushing behavior of Aluminum/Cfrp hybrid tubes with circular-hole triggering mechanism. Thin-Walled Structures 2023; 182: 110321.
37. Stephens, MA. Edf statistics for goodness of fit and some comparisons. Journal of the American statistical Association 1974; 69(347): 730–37.
38. Jehad, AMF, Al-Sherrawi, MH. Performance of RC beams reinforced with steel fibers under pure torsion. Engineering, Technology & Applied Science Research, 2024; 14(5): 16142–16147. https://doi.org/10.48084/etasr.7687